electronic reprint

Acta Crystallographica Section D
Biological Crystallography
ISSN 0907-4449

Low-temperature water reconstruction in concanavalin A, with implications for controlled protein crystal annealing

Sean Parkin and Håkon Hope

Acta Crystallographica Section D
Biological Crystallography
ISSN 0907-4449

Low-temperature water reconstruction in concanavalin A, with implications for controlled protein crystal annealing

Sean Parkin[a]* and Håkon Hope[b]

[a]Department of Chemistry, University of Kentucky, Lexington, KY 40506-0055, USA, and [b]Department of Chemistry, University of California, Davis, CA 95616, USA

Correspondence e-mail: spark2@uky.edu

Received 1 July 2003
Accepted 17 September 2003

Flash-cooled crystals of the *I*222 form of concanavalin A undergo a sharp non-destructive non-reversible phase transition upon warming to between 160 and 165 K, characterized by an anomalous increase in unit-cell volume. The expansion is anisotropic and primarily affects the *b* and *c* axes. Three sets of 1.7 Å X-ray diffraction data were collected from one crystal: immediately after flash-cooling (130 K), after slow warming to 170 K and after re-cooling to 130 K. Measurable changes in reflection width after the transition were apparent. Each data set was collected under very similar conditions (aside from temperature). Structures refined against each data set using a powerful phase-bias reduction algorithm indicate negligible rearrangement of the protein molecule and its first hydration shell. Further away from the protein surface, on the edge of the fully disordered solvent regions, a small number of more dramatic changes were apparent. Little is known about the behaviour of water confined within dimensionally restricted spaces, but solvent cavities and channels in protein crystals provide a rich source of reproducible nanoscale water assemblies. This paper presents information on the behaviour of water confined within protein cavities in relation to the physics of protein crystal annealing.

1. Introduction

Most high-quality diffraction data are now collected at cryogenic temperatures. Given appropriate experimental techniques, low temperature can improve signal-to-noise ratios by reducing thermal motion (Parkin *et al.*, 1996*a*,*b*; Hope, 1988; Tilton *et al.*, 1992), extend resolution (Hope, 1988; Rodgers, 1994), resolve disorder (Parkin *et al.*, 1996*a*), allow better definition of water structure (*e.g.* crambin; Teeter & Hope, 1986) and dramatically reduce radiation damage (Low *et al.*, 1966; Haas & Rossmann, 1970; Dewan & Tilton, 1987; Hope *et al.*, 1989). Data from just one crystal are generally better than data from many crystals because scaling and merging of multiple data sets is eliminated. Nevertheless, flash-cooling can increase reflection-profile widths and compromise the attainable resolution. Many problems associated with low-temperature work can be alleviated by strict experimental control, but this is not always practical or possible. Until recently, conventional wisdom held that thawing would inevitably destroy a flash-cooled crystal. Despite mounting evidence to the contrary, this idea persisted even after reports of successful protein-crystal annealing (Harp *et al.*, 1997, 1998; Yeh & Hol, 1998). We now know that under appropriate well defined conditions, warming to room temperature and re-cooling can dramatically improve diffraction. Annealing is now an established means of improving data quality and even of resurrecting apparently worthless crystals (Harp *et al.*,

1998). Recent work has begun to shed light on the mechanisms of protein-crystal annealing (Kriminski *et al.*, 2002).

The key to understanding low-temperature protein-crystal phase transitions lies in the bulk solvent. Little is known about such water in protein crystals, but there is a large body of work concerned with pure water at low temperature (*e.g.* Angell, 1995; Mishima & Stanley, 1998; Velikov *et al.*, 2001). Several forms of solid amorphous water have been reported; their physical properties depend on their method of preparation (Debenedetti & Stanley, 2003). A complex nomenclature has evolved, including low-density amorphous (LDA), high-density amorphous (HDA), amorphous solid water (ASW) and hyperquenched glassy (HGW) water (Narten *et al.*, 1976; Mishima *et al.*, 1984, 1985; Mishima & Stanley, 1998; Velikov *et al.*, 2001). One view is that solid supercooled water (*i.e.* 'glassy' or 'vitreous' ice) undergoes a glass transition, $T_g = 136$ K, to a highly viscous liquid (HVL), which crystallizes into cubic ice (I_c) on warming to 155 K (Weik *et al.*, 2001). The value of T_g is controversial, however. In experiments on HGW, Velikov *et al.* (2001) propose $T_g = 165$ (5) K and suggest that vitreous pure water remains glassy until it crystallizes between 150 and 160 K. A third form, identified as 'vitreous water' and as 'amorphous solid water' (ASW; Johari *et al.*, 1996), is almost indistinguishable from HGW (Mayer, 1985; Angell, 2001). Whether the physics of pure water is directly transferable to water within protein crystals is, of course, not known. Protein crystals grow from complex mixtures of salts, buffers and organic precipitants, which alter physical properties such that ice nucleation may be depressed below T_g (Angell, 2002). Many atomic resolution protein structures incorporate well ordered cryoprotectant molecules, which implies that water in protein crystals is different from pure water. Moreover, Velikov *et al.* (2001) suggest that water held in nanoscopic assemblages does not behave like pure water.

Analysis of disordered water in protein crystals is difficult because it is amorphous. This is compounded in many experiments by polycrystalline ice diffraction, which can obscure the origin of ice formation. Here, we describe a phase transition in flash-cooled crystals of concanavalin A (conA; Parkin, 1993) and explain the anisotropic unit-cell expansion in terms of the geometry and orientation of water channels using data collected before and after the phase transition from the same crystal. The results limit the range of acceptable explanations for phase transitions that occur in protein crystals at low temperature.

2. Materials and methods

2.1. Crystallization, crystal cooling and mounting

Large (typically 0.1–0.25 mm^3) well faceted crystals of the *I*222 form of conA (Sigma, St Louis, MO) grew at pH 6.5 using the dialysis method described by Kalb *et al.* (1988). Prior to cooling, crystals were transferred to an antifreeze solution of reservoir buffer diluted with ~30% 2-methyl-2,4-pentanediol (MPD), washed and inspected for ~30 s. They were mounted in fibre loops on copper mounting pins and cooled directly in a cold nitrogen stream at either 120 or 130 K using standard techniques (Parkin & Hope, 1998).

2.2. Unit-cell *versus* temperature measurements

A crystal was indexed at 120 K from eight reflections in the range $5 < 2\theta < 15^\circ$ (Cu $K\alpha$ radiation, Siemens P4RA serial diffractometer). Unit-cell parameters were refined in a least-squares fit of $\sin^2\theta$ values for 24 intense reflections ($40 < 2\theta < 45^\circ$) well distributed in reciprocal space (all Laue equivalents). The temperature was lowered to 95 K and the cell was re-refined against the same 24 reflections. Unit-cell parameters were obtained at 5 K increments up to 180 K. At each step, temperature equilibration took ~5 min and reflection centering took ~15 min. An abrupt jump in unit-cell volume between 160 and 165 K was observed (Fig. 1). As a check, the temperature was lowered, first to 160 K and then to 155 and 120 K, where redetermination of the unit cell (*i.e.* after the transition) was consistent with the volume jump. Unit-cell parameters were then redetermined at 175 and 180 K. Similar measurements were made for two other crystals from different growth batches. Above 180 K, diffraction quality began to degrade and further measurements were abandoned, although the crystals remained clear. Apart from slight variations in unit-cell parameters, the trends with temperature were the same. A fourth crystal, which was flash-cooled, warmed through the transition and held at 180 K on an ADSC multiwire system, remained clear and showed no evidence of ice-ring formation on diffraction data frames. Experiments using drops and thin films of antifreeze also showed no evidence of sharp ice-ring formation.

2.3. Data collection before and after the transition

Diffraction data were collected using twin ADSC multiwire detectors from a fifth crystal (flash-cooled to 130 K) in nine 30° ω scans to ~1.61 Å over 6 d. Symmetry equivalents ($\varphi + 180^\circ$; $-\chi$) were collected with faster scans (~25 h) in order to account for overloads and to provide Friedel-related

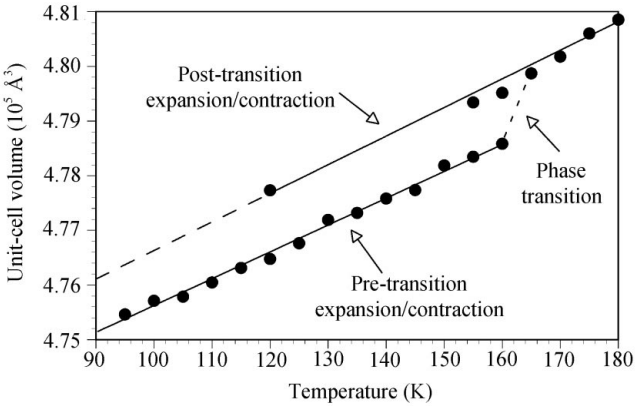

Figure 1
Unit-cell expansion/contraction for *I*222 conA as a function of crystal temperature. Least-squares fit lines are drawn through pre- and post-transition data points. Note the abrupt jump in unit-cell volume between 160 and 165 K.

Table 1
Crystal and data-collection statistics.

Values in parentheses are for the highest resolution shell (1.8–1.7 Å).

	Set 1 (130 K)	Set 2 (170 K)	Set 3 (130 K)
Unit-cell parameters†			
a (Å)	62.28	63.37	62.30
b (Å)	86.25	86.50	86.42
c (Å)	89.25	89.40	89.36
Resolution (Å)	1.7	1.7	1.7
No. of data‡	49680	38822	49680
Completeness§ (%)	98 (96)	98 (96)	98 (96)
Multiplicity	4.4	2.3	4.4
$\langle I/\sigma(I)\rangle$	26.7 (8.7)	17.6 (5.5)	26.9 (10.3)
$R_{\rm merge}$ (%)	4.0 (8.38)	3.7 (10.0)¶	3.6 (9.0)
Mosaicity†† (°)	0.45	0.50	0.40

† The unit-cell parameters (for crystal 5) used in refinement are averages of the values optimized from each scan of multiwire diffraction data. They are neither as accurate nor as precise as the serial diffractometer data given for crystal 1 (§§2.2 and 3.1). ‡ Friedel pairs not merged (see Flack & Bernardinelli, 1999, 2000). § Completeness is calculated after merging of Friedel-related reflections. ¶ $R_{\rm merge}$ values for set 2 appear comparable to those for sets 1 and 3, but the merging was over half the number of scans. See Diederichs & Karplus (1997). †† Here 'mosaicity' is used in a broad sense to describe the average FWHM of reflection profiles.

measurements. The crystal was then warmed slowly to 170 K. To ensure sufficient time above the transition point to re-establish equilibrium, the crystal was held at 170 (1) K for 1 d while the symmetry-equivalent scans were repeated. Finally, the crystal was re-cooled slowly back to 130 (1) K and the full data-collection procedure was repeated. Other than temperature and the effects of the phase transition, the conditions for the two 130 K data sets were the same. The 170 K data are weaker and lack the Friedel-related scans. Crystal orientation and temperature were controlled over the full 16 d of data acquisition. Periodic inspection of the crystal and diffraction pattern showed no evidence of ice formation.

Data were processed with the ADSC multiwire suite and were scaled and merged using *XtalView* (McRee, 1992) and *XPREP* (Sheldrick, 2001). Friedel opposites were kept separate throughout. Three data sets, corresponding to the pre-transition structure at 130 K (set 1) and the post-transition structure at 170 (set 2) and 130 K (set 3), were created. Since coverage between 1.61 and 1.70 Å was low, the data were truncated at 1.70 Å in order to ensure adequate completeness. As a result of the small unit-cell parameter changes, sets 1 and 3 required some additional pruning to reduce them to a common set of indices. No further editing of the 170 K data set was performed. Coverage, intensity and reflection statistics are given in Table 1.

2.4. Structure solution and refinement

Atomic coordinates were taken from the 1.2 Å PDB entry 1jbc (Parkin *et al.*, 1996*b*). Rigid-body refinements followed by restrained least-squares refinements with *SHELXL*93 (Sheldrick, 1997) did not reveal any substantial differences between the two 130 K structures. Extensive omit-map model rebuilding and further least-squares refinements again showed no significant differences in the protein molecule itself.

It is well known that model phases can bias non-centrosymmetric structure refinements towards the starting model (Hodel *et al.*, 1992; Kleywegt, 2000), but modern phase-bias reduction can give dramatic results (Perrakis *et al.*, 1997; Terwilliger, 2000). Since we expected very subtle structure changes, some form of phase-bias removal was essential. To this end, 'prime-and-switch' phasing (Terwilliger, 2001) was performed after removal of all water from the models. Briefly, high-quality (*e.g.* σ_A-weighted; Read, 1986) but nevertheless biased phases are used to initiate phasing from the phase-probability distributions of an electron-density map-likelihood function. Final phases from the map-likelihood function alone show minimal bias toward the starting set. In practice, precise but biased phases yield new phases with reduced bias (*i.e.* more accurate) but increased noise (*i.e.* less precise).

To further minimize bias and hence to increase the chances of identifying real structural changes, the protein molecules and the solvent regions for the 130 K pre-transition (model 1) and post-transition (model 3) data sets were rebuilt independently and automatically using *Xfit*4.0 (*XtalView*; McRee, 1992) from prime-and-switch phased maps. These models, with 173 and 177 water molecules, respectively, were subjected to further automated water rebuilding (*SHELXWAT*; Sheldrick, 1997). Protein bonds were restrained either to standard values (Engh & Huber, 1991) or to adjustable parameters. The type of restraint for any given bond length or angle was the same for all models. Models 1 and 3 converged at about the same rate to similar values of R_1 and $R_{\rm free}$ (the $R_{\rm free}$ subsets had identical indices), with very similar protein coordinates and about the same number of water molecules. After completion of refinement of the two 130 K models, the same treatment was applied to the 170 K post-transition data (model 2). Refinement statistics are given in Table 2.

Table 2
Refinement statistics.

	Model 1 (130 K)	Model 2 (170 K)	Model 3 (130 K)
$R_{\rm work}$† (%)	14.68 (15.54)	14.72 (15.39)	14.76 (15.35)
$R_{\rm free}$† (%)	18.85 (19.79)	18.67 (20.03)	18.87 (19.70)
No. water molecules‡	268 (54)	274 (44)	280 (52)
$\langle B\rangle_{\rm protein}$ (Å^2)	16.7	17.0	16.2
$\langle B\rangle_{\rm water}$ (Å^2)	30.1	30.7	29.6

† Values are given for data with $I > 2\sigma(I)$ and for all data in parentheses. ‡ The number of half-occupancy water molecules is given in parentheses.

3. Experimental results

3.1. Unit-cell parameters

Least-squares fit unit-cell parameters from carefully chosen well centered reflections on a four-circle serial diffractometer are generally more accurate than those obtained from area-detector data. Immediately after flash-cooling to 120 K, the unit-cell parameters were a = 62.07 (2), b = 86.15 (3), c = 89.11 (3) Å and V = 476 500 Å^3 (§2.2). At 95 K, the unit cell contracted by ∼1000 Å^3. Upon warming in 5 K increments to 160 K, the unit-cell volume increased in a linear (R^2 = 0.994)

fashion by ∼1% per 100 K. Between 160 and 165 K, however, the unit-cell volume underwent a non-reversible increase of ∼1300 Å^3, equivalent to more than 5% per 100 K. The unit-cell expansion was not uniform. The *a* axis underwent linear expansion (R^2 = 0.991) from 62.001 (17) Å at 95 K to 62.249 (19) Å at 175 K, but there was no further increase from 175 to 180 K. Post-transition, on cooling back to 120 K, the *a* axis was slightly longer than its pre-transition length, but not by a significant amount (Fig. 2*a*). In contrast, the *b* and *c* axes showed an abrupt increase between 160 and 165 K (Figs. 2*b* and 2*c*). The pre-transition expansion/contraction rates for *b* and *c* were smaller than those for *a*.

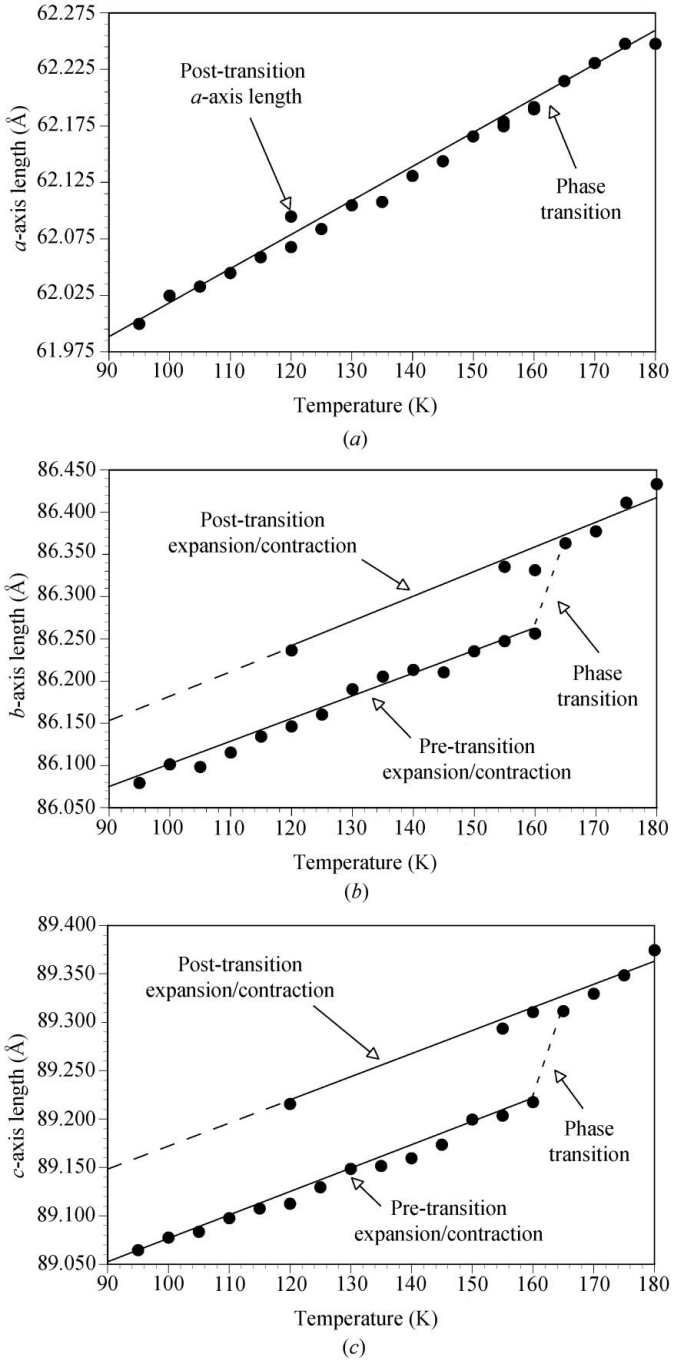

Figure 2
Expansion and contraction of the (*a*) *a* axis, (*b*) *b* axis and (*c*) *c* axis for *I*222 conA as a function of temperature. Least-squares fits are drawn through pre- and post-transition data points. Note the absence of any jump in the *a* axis, in contrast to the behaviour of both the *b* and *c* axes.

3.2. Crystal- and data-quality statistics

Crystal and data quality are usually assessed by resolution, mosaic spread, completeness, signal-to-noise ratio and merging statistics. The crystal was of high quality; it diffracted to ∼1 Å resolution, with single-peaked reflections well separated from their neighbours.

The angular width of diffraction maxima contains contributions from many sources other than mosaic spread, as defined by Darwin (1923). Nevertheless, 'mosaicity' has become a catch-all descriptor that is often taken as the measured reflection width. Reflection widths were calculated from the processed multiwire frames, which are well suited to extraction of such profiles. At 130 K (pre-transition), the average FWHM was 0.45°. At 170 K (*i.e.* post-transition) it was 0.50° and it was 0.40° upon cooling back to 130 K.

Signal-to-noise ratios and merging statistics as a function of resolution are only directly comparable for data sets 1 and 3, because data set 2 was collected at a faster scan rate. In terms of commonly used statistics, there is little difference between the two 130 K sets. Set 1 is slightly weaker at low resolution and marginally stronger at high resolution. Merging statistics are marginally better for set 3 for all but the highest-resolution shell. Merging statistics between the three data sets suggest very similar structures. The $R_{\rm merge}$ value for sets 1 and 2 together was highest, at 5.68%; between sets 1 and 3 $R_{\rm merge}$ was 4.29% and between sets 2 and 3 it was 3.29%. This result is largely as expected: sets 1 and 2 differ both in temperature and by the effects of the phase transition. Despite the similarity of Bragg intensities, the broad solvent-diffraction rings were slightly different after the phase transition. All three data sets gave a broad background ring, but for set 1 this ring had a

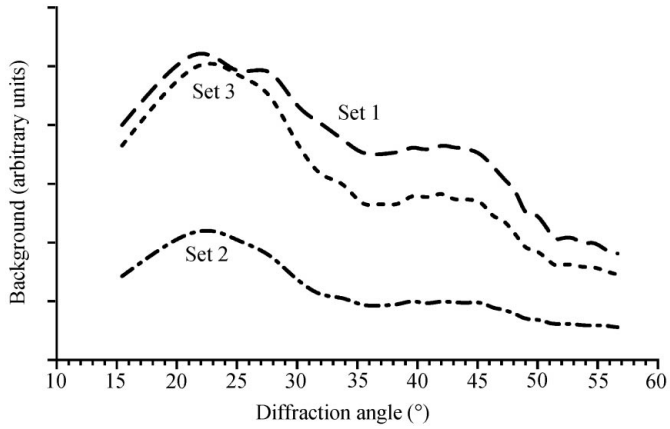

Figure 3
Average backgrounds for data sets 1 (pre-transition, 130 K), 2 (post-transition, 170 K) and 3 (post-transition, 130 K). Note the shoulder in set 1 at ∼27° 2θ (∼3.3 Å). In sets 2 and 3, this shoulder is greatly diminished. Backgrounds are lower in set 2 because this data set was collected much more rapidly.

shoulder at ∼3.3 Å. After the transition, this shoulder was diminished (Fig. 3).

3.3. Structural information

The structure of conA is well known (Reeke *et al.*, 1971; Hardman *et al.*, 1971; Becker *et al.*, 1975; Parkin *et al.*, 1996*b*; Deacon *et al.*, 1997). Given the similarity of all three data sets, structural rearrangements during the phase transition are expected to be small. To simplify the description, comparison is restricted to models 1 and 3 except where stated otherwise. There is a uniform shift of the whole protein molecule in the *bc* plane by ∼0.12 Å, with negligible movement along *a*. The best rigid-body superposition (Kearsley, 1989; Parkin, 1996) of model 1 onto model 3 required rotation of less than 0.1°, no movement along *a* (0.004 Å calculated), but translations of 0.108 and 0.057 Å along *b* and *c*, respectively. Comparison of mean atom shifts and r.m.s. atom shifts conveys more information. For the protein atoms alone, the mean coordinate shift parallel to *a* was 0.007 Å, but the r.m.s. shift was 0.039 Å, indicating that shifts parallel to *a* were random. For movement parallel to *b* and *c*, however, the mean coordinate shifts of 0.109 and 0.055 Å, respectively, are similar to the r.m.s. shifts of 0.112 and 0.064 Å, indicating a systematic movement in the *bc* plane.

To simplify the description, it is convenient to split the water substructure into three groups. Water in the first coordination shell (type 1) is hydrogen bonded or in close proximity to protein; type 2 water, in higher solvation shells, is still ordered enough to be found in electron-density maps; lastly, fully disordered solvent is further removed from the protein. There was a small increase in the number of refinable water positions after the transition, even at the higher temperature, and a slight decrease in *B* values at 130 K (Table 2). Overall, however, solvent structures refined at 1.7 Å in this work were very similar to those at atomic resolution (Parkin *et al.*, 1996*b*; Deacon *et al.*, 1997).

The mean *versus* r.m.s. shifts for type 1 water parallel to the *a*, *b* and *c* axes were −0.010 *versus* 0.099 Å, 0.095 *versus* 0.154 Å and 0.051 *versus* 0.093 Å, respectively. Thus, type 1 water shifts are random along *a* and systematic in the *bc* plane, largely in concert with the protein molecule. The behaviour of type 2 water, however, is different. Mean shifts parallel to *a*, *b* and *c* for these water molecules were −0.025, 0.041 and 0.036 Å, respectively, indicating greatly reduced systematic movement in the *bc* plane. Furthermore, the r.m.s. shifts of type 2 water molecules were much higher, at 0.196, 0.189 and 0.185 Å for *a*, *b* and *c* axes, respectively. It is of significance that r.m.s. shifts parallel to *a* for type 2 water are comparable with the shifts associated with *b* and *c*. A small number of type 2 water molecules shift by as much as 1 Å or more parallel to the *a* axis (Fig. 4). An obvious caveat is that type 2 water molecules tend to correspond to smaller more diffuse features of electron-density maps. The displacement parameters of these molecules are larger and their coordinates are less well defined than those of type 1. Nevertheless, the trend is clear. Coordinate precision estimates for 'average' atoms calculated a number of ways (Cruickshank, 1999; Blow, 2002) are about 0.06 Å. For type 2 water molecules in general, coordinate precision will be somewhat worse, but still an order of magnitude smaller than some of the observed shifts. Disordered bulk water represents more of a challenge (§4.1) because it cannot be found and refined in the same way as ordered water.

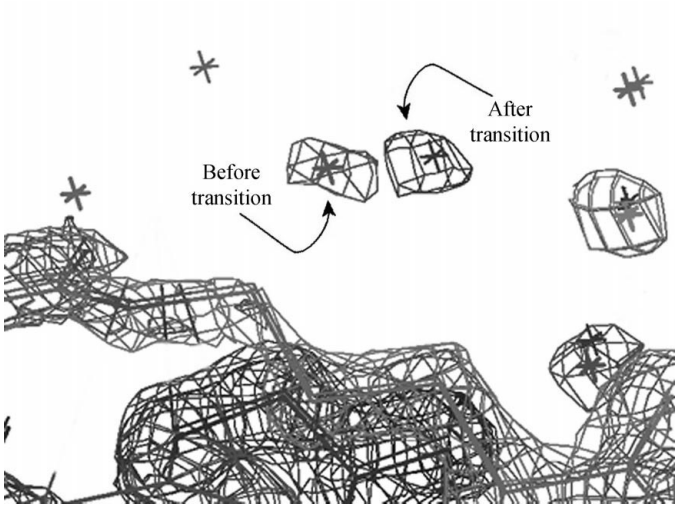

Figure 4
Superposition of a section of type 2 (*i.e.* second and higher solvation shell, weak electron density, some disorder) water molecules in models 1 and 3. The *a* axis is roughly horizontal. The two electron-density cages in the middle of the figure are for the same water molecule before (left) and after (right) the phase transition; the shift was ∼1.4 Å along the *a* axis. The water positions indicated without electron-density cage contours are difference-map peaks for which electron density is absent at this contour level.

4. Discussion

Anisotropic changes in unit-cell parameters upon cooling are common in small molecules and have been reported for protein crystals. The *c* axis of bovine pancreatic trypsin inhibitor (BPTI) lengthens on cooling to 125 K from 74.1 (Wlodawer *et al.*, 1984) to 75.39 (3) Å (Parkin *et al.*, 1996*a*), despite a volume contraction of ∼3%. Weik *et al.* (2001) report anomalous unit-cell expansion at ∼155 K for flash-cooled trigonal crystals of *Torpedo californica* acetylcholinesterase (*Tc*AChE) and crystals of β_2-glycoprotein I (β2gpI), but not for orthorhombic *Tc*AChE. Unit-cell volumes were larger at 180 K than at 105 K, by ∼3.7 (1)% for trigonal *Tc*AChE and ∼7.5 (3)% for β2gpI. Of more comparative value, however, is the relative expansion as a result of phase transition, *i.e.* for unit-cell volumes measured at the same temperature. This expansion can be estimated from Fig. 1 of Weik *et al.* (2001) as ∼1–3% for trigonal *Tc*AChE and β2gpI, which is larger than the increase observed for conA (∼0.25%) at a slightly higher temperature (160–165 *versus* 155 K). These unit-cell expansions correlate loosely with solvent content (68% for trigonal *Tc*AChE, 86% for β2gpI and 42% for conA), which may be a factor in determining the onset temperature of phase transition.

4.1. Anisotropic unit-cell expansion

A reasonable explanation for the observations is that rapid cooling arrests a metastable state for the bulk water, which transforms to a stable low-temperature form upon phase transition (Parkin, 1993). In *I*222 conA, this process does not alter the protein itself or the water closely associated with it, so it is safe to conclude that the phenomenon is primarily associated with bulk water. Projections along the unit-cell axes (Fig. 5) reveal channels parallel to *a* that are ∼30–40 Å across. Along *b* there are no channels, while along *c* there are much narrower (∼10 Å) channels. The arrangement of disordered water within protein crystal cavities is not known and differences may exist between crystals of the same protein. Nonetheless, solvent-diffraction rings are broad and diffuse, indicative of an isotropic amorphous phase.

The effect on the protein crystal as a whole is far from isotropic. If the crystal is considered as interpenetrating substructures of protein and water (Kriminski *et al.*, 2002), then the measured unit-cell parameters give the periodicity of the protein substructure. Water is able to expand unhindered along channels parallel to *a*, but parallel to *b* expansion requires the protein molecules to be forced apart in a similar manner to the view presented by Weik *et al.* (2001). The smaller channels along *c* are consistent with the smaller atom shifts observed along *c* relative to *b*. Other evidence lies in the large r.m.s. shift parallel to *a* for type 2 water as a whole and the small number of shifts by 1 Å or more parallel to *a* for some water molecules on the edge of the channels. These water molecules may have experienced a buffeting motion parallel to *a* caused by expansion within the solvent channels.

4.2. Phase transitions and annealing of water structure at low temperature

4.2.1. On the origin of ice rings in annealed crystals. Weik *et al.* (2001) observed ice-diffraction rings for three different crystals which were each cooled in mineral oil in the same way. Ice rings from two crystals were attributed to crystallization of water within channels, whereas ice in the orthorhombic *Tc*AChE, which possesses solvent pools rather than channels, was attributed to crystallization of surface water. While this scenario is possible, the analysis is inconsistent. The notion of

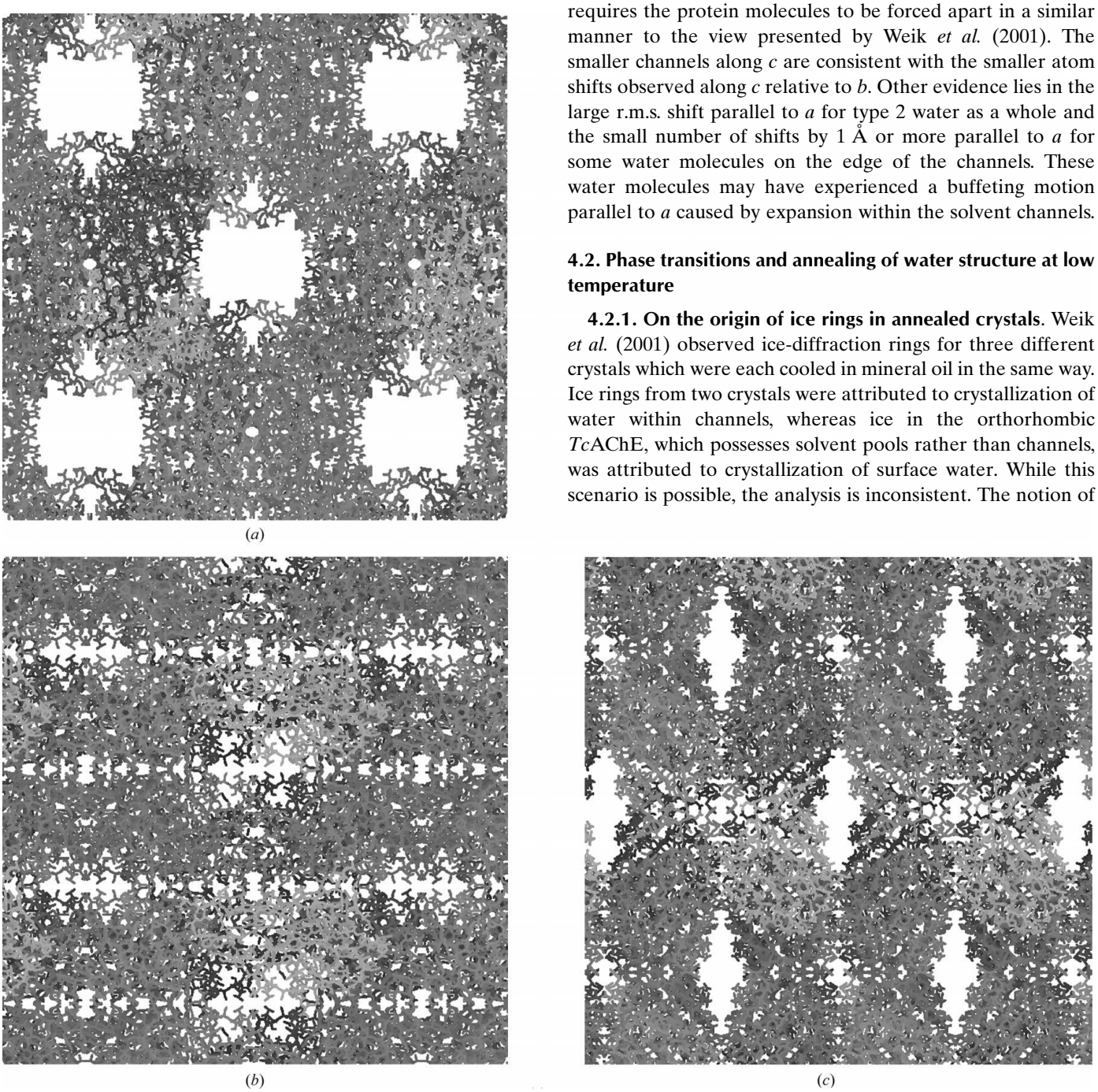

Figure 5
Packing diagrams viewed along the (*a*) *a* axis, (*b*) *b* axis and (*c*) *c* axis, showing the solvent channels (∼30 Å) that run the length of the crystal parallel to *a*, the absence of channels parallel to *b* and the much narrower (∼10 Å) channels parallel to *c*.

ice formation within channels that does not destroy the protein framework is not intuitive. One would expect more destruction for higher water content because of the large volume increase on phase transition and the weakness of protein–protein interactions. Although crystallite sizes limited by solvent-channel geometry to ∼60 or ∼80 Å would give relatively narrow powder-diffraction line widths of ∼1–2° with Cu $K\alpha$ radiation (Scherrer, 1918), the similar handling of each crystal suggests the same origin of the ice in each. Thus, it is likely that the ice rings observed for all three crystals of Weik *et al.* (2001) arose at least in part from crystallization of surface water. Indeed, Weik *et al.* (2001) report ice formation at ∼155 K for droplets of antifreeze solution used for both forms of *Tc*AChE. Surface-nucleated ice that propagates into a crystal would likely cause damage (Parkin & Hope, 1998) and some degradation is noted by Weik *et al.* (2001), but the extent is unclear. Interestingly, the antifreeze for β2gpI did not form ice below ∼170 K, but the presence of foreign bodies can affect solution properties. In related work, the onset of diffuse ring sharpening in antifreeze droplets has been found to depend on the presence of heterogeneous nucleation sites, including dirt and denatured protein. It may also be affected by the crystal surface. Surface-nucleated ice would obscure other sources of ice and obfuscate definitive assignment of its origin. An alternative scenario (Kriminski *et al.*, 2002) is that internal ice originates in water trapped at dislocations and grain boundaries. Optimal cooling of some crystals requires incubation in a stabilization solution prior to cryoprotection and this is likely to be related to the removal or modification of such water. Carefully controlled dehydration has produced distinct lower solvent-content forms of the same crystal structure (Pelletier & Kraut, 1992; Schick & Jurnak, 1994; Esnouf *et al.*, 1998). Kriminski *et al.* (2002) proposed that because LDA expands on cooling, a slow enough cooling rate could cause water to squeeze out and accumulate at the crystal surface. Similar arguments can be made for expansion during the phase transitions observed here and by Weik *et al.* (2001). With oil as a cryoprotectant, there would be little to prevent surface water from crystallizing. In light of the lack of ice-ring formation in conA and the ambiguous origin of ice rings observed by Weik *et al.* (2001), the evidence for transformation to crystalline ice requires further scrutiny.

4.2.2. Protein crystal water and pure water. Pure liquid water gives a broad diffraction ring at ∼3.2 Å (Dorsey, 1940), whereas the vitreous 'ice' of Dowell & Rinfret (1960) gave a broad ring at ∼3.7 Å and polycrystalline cubic ice gives a sharp ring at 3.67 Å. In diffraction studies of ASW, an extra feature at ∼3.3 Å has been suggested to result from a higher density form (Narten *et al.*, 1976). Diffraction rings are characteristic of structural features and may be shifted by additives. For example, Mitchell & Garman (1994) report ice rings at 4.2 Å for a non-optimal glycerol concentration. After the conA phase transition, diffraction rings are still broad with no evidence of directionality and thus the phase change in the bulk solvent is completely isotropic. Analysis of the diffraction-pattern background noise reveals broad ring structures for the three conA data sets, with an additional shoulder at ∼3.3 Å (Fig. 3) in set 1. Diffuse water diffraction in each would have contributions from internal water and cryoprotectant, but this crystal was mounted in ∼30% MPD, which is known to suppress ice formation over a range of conditions (Parkin *et al.*, 1996*b*; Deacon *et al.*, 1997; Rodgers, 1997). Diffuse diffraction from the cryoprotectant alone was very similar at 90, 130 and 170 K. Narrowing of the ring did not occur until ∼185 K, consistent with degradation of the diffraction pattern above 180 K. Differences between backgrounds before and after phase transition can therefore be traced to structure changes within the crystal itself.

The abrupt volume increase and the disappearance of the shoulder at ∼3.3 Å are consistent with more than one mechanism. Since pure liquid water gives a broad diffraction ring at ∼3.2 Å and ASW exhibits an extra ring at ∼3.3 Å (Narten *et al.*, 1976), the observed shoulder at ∼3.3 Å could arise from a phase similar to either ASW or HGW. The volume jump is consistent with either a transition between amorphous states or a transition between an amorphous state and some form of nanocrystalline ice. Since HDA and LDA have been shown to coexist (Suzuki & Mishima, 2000), a transition from HDA to LDA is possible (Johari *et al.*, 1996; Mishima & Stanley, 1998; Velikov *et al.*, 2001). Velikov *et al.* (2001) suggest that crystallization occurs directly at ∼150–160 K from HGW, without an intermediate highly viscous liquid (HVL) phase. LDA contracts on warming from 30 to 150 K (Kriminski *et al.*, 2002), so the volume increase is also consistent with transformation of LDA to nanocrystalline cubic ice at temperatures of ∼155 (Weik *et al.*, 2001) or 160–165 K (this work), with or without an HVL intermediate. These temperatures are comparable to the crystallization temperature of pure vitreous water (∼150–160 K; Johari *et al.*, 1996; Velikov *et al.*, 2001), but additives can stabilize a given phase (Angell, 2002).

4.2.3. Water-structure phase transition in annealed protein crystals. Expansion of water along solvent channels cannot be measured, so the volume increase is a poor indicator of density changes within them. The view proposed by Kriminski *et al.* (2002) of competing influences of expansion/contraction for protein and water substructures is supported by Fig. 1(*c*) of Weik *et al.* (2001), which clearly shows a contraction for β2gpI between ∼110 and ∼145 K. This behaviour would surely be more pronounced for high-solvent-content crystals if some component of the water phase contracted on warming (as in LDA).

In conA, a transition to polycrystalline ice is possible only if the solvent regions are much more restrictive of crystallite size than the channel diameter. For particles limited to ∼30 Å, the Scherrer (1918) equation suggests powder-diffraction line widths (FWHM) of ∼2.5°, *i.e.* much narrower than those observed for conA. A FWHM of ∼10° is closer to the mark and implies particle sizes of ∼10 Å. Kriminski *et al.* (2002) note that the protein surface can influence hydrogen bonding over ∼10 Å. Thus, a ∼30 Å diameter channel would have a column of water free from the influence of protein only ∼10 Å across, safely within the range of nanoscale line broadening. In experiments on tetragonal lysozyme (∼42% water, ∼20 Å diameter channels along *c*) and triclinic lysozyme (∼26%

water) by Kriminski *et al.* (2002), *in situ* annealing to temperatures as high as 250 K consistently improved reflection width and resolution for some well defined annealing times. Diffraction quality for tetragonal lysozyme was observed to degrade at ~268 K; this degradation could have been caused by ice formation, but there was no particular mention of ice at any specific temperature *per se*. In any event, the lack of evidence of crystalline ice in conA and the inconsistent interpretation of Weik *et al.* (2001) suggest that the case for a transition to cubic ice is not proven and that the more intriguing case of a first-order transition between amorphous states is possible (Angell, 2003).

Whether the effects seen for conA, *Tc*AChE and β2gpI are initiated within the crystal or at the surface remains to be determined. If the cause is internal, then the trigger could be the point where expanding protein and contracting water substructures induce sufficient strain as to finally become incompatible. The lack of an abrupt volume jump in orthorhombic *Tc*AChE, however, suggests that channels are necessary for phase transition, presumably because of their connection with the crystal surface. The behaviour of orthorhombic *Tc*AChE thus adds weight to the likelihood of surface nucleation and propagation into the crystal along solvent channels.

4.3. Implications for controlled protein-crystal annealing

Ice formation on flash-cooling is usually a symptom of non-optimal cooling conditions (Hope, 1988; Mitchell & Garman, 1994) or poor experimental geometry (Parkin & Hope, 1998). A common observation during optimization of cooling conditions is that the three powder rings of hexagonal ice at 3.90, 3.67 and 3.44 Å coalesce with increased antifreeze into a broader single ring at 3.67 Å. Further broadening of this ring is characteristic of ice suppression. A better understanding of liquid and solid water would help to clarify water-in-crystal phase transitions, but it is not totally necessary. Phase transitions that result in polycrystalline ice are unlikely to produce acceptable annealing protocols.

Several schemes for annealing protein crystals have been reported. The best known requires removal of a crystal from a cold stream to a drop (~0.3 ml) of cryoprotectant. A 3 min incubation is followed by re-flash-cooling (Harp *et al.*, 1998). A second method involves a few cycles of *in situ* thawing and rapid cooling (Yeh & Hol, 1998). To explain the structural basis of annealing-induced improvements, Kriminski *et al.* (2002) developed a third method. This involves the relatively rapid warming of a cold crystal to either ~230 or ~250 K (*i.e.* well below thawing temperatures) for 5–10 s, which is achieved by dynamically mixing cold and warm gas flows, but the authors note a lack of reproducibility in their warming and re-cooling rates. The controlled warming described in this work, however, has more in common with that described by Weik *et al.* (2001). Slow warming can be achieved with remarkable precision, so it is easy to exercise total control over the crystal environment. Although it was not originally intended as a means of annealing protein crystals, the modest improvement in average reflection widths for conA indicates greater long-range order after the phase transition. Automated refinement also gave slightly more water sites in the post-transition model and average *B* values were slightly reduced for both protein and water atoms.

5. Conclusion

Anisotropic expansion in a low-temperature phase transition in the *I*222 form of concanavalin A is explained by the influence of water channels. The abrupt volume jump is a consequence of a phase transformation within the bulk-solvent region from its flash-cooled glassy state to either a lower density amorphous phase or nanocrystalline ice. The effect is anisotropic because expansion along water channels can occur without interfering with protein molecules, but expansion across the channels requires the protein molecules to be forced apart. Given similar observations by Weik *et al.* (2001), it is likely that this phenomenon is general for protein crystals with solvent channels. The physical properties of water at low temperature are complex and the extent to which its behaviour is altered by additives is unknown. Nevertheless, it is clear that flash-cooling has the effect of arresting a metastable state, which transforms to a more stable low-temperature form on phase transition. Despite the importance of low-temperature water behaviour, the exact nature of the phase transition is less important in protein crystallography than the observation that certain characteristics of protein-crystal diffraction can be improved. Slow warming resulted in a small decrease in reflection widths and an absence of ice rings for conA. Where ice formation can be reliably kept in check, it constitutes a fully controllable annealing protocol. Although intensity statistics and refined structural parameters for these already superb crystals show little overall change, automated refinement resulted in more water sites after the transition. A more representative test for typical proteins would involve crystals that do not diffract to atomic resolution.

SP thanks the University of California for a Regents Fellowship during the time that the phenomenon described in this paper was discovered. We also thank Tom Terwilliger (*RESOLVE*), Eleanor Dodson (CCP4) and Chris Nielsen (multiwire data archives). Some of the diffraction data were collected under the auspices of the US Department of Energy at LLNL under contract No. W-7405-ENG.

References

Angell, C. A. (1995). *Water: A Comprehensive Treatise*, edited by F. Franks, Vol. 7, pp. 1–81. New York: Plenum.
Angell, C. A. (2001). *Water Science for Food, Health, Agriculture and the Environment*, edited by Z. Berk, R. B. Leslie, P. J. Lilford & S. Mizrahi, pp. 1–30. Lancaster, PA, USA: Technomic Publishing Co.
Angell, C. A. (2002). *Chem. Rev.* **102**, 2627–2649.
Angell, C. A. (2003). Personal communication.
Becker, J. W., Reeke, G. N. Jr, Wang, J. L, Cunningham, B. A. & Edelman, G. M. (1975). *J. Biol. Chem.* **250**, 1513–1524.
Blow, D. M. (2002). *Acta Cryst.* D**58**, 792–797.
Cruickshank, D. W. J. (1999). *Acta Cryst.* D**55**, 583–601.

Darwin, C. G. (1923). *Philos. Mag.* **43**, 800–829.
Deacon, A., Gleichmann, T., Kalb, A. J., Price, H., Bradbrook, G., Yariv, J. & Helliwell, J. R. (1997). *J. Chem. Soc. Faraday Trans.* **24**, 4305–4312.
Debenedetti, P. G. & Stanley, H. E. (2003). *Phys. Today*, **56**, 40–46.
Dewan, J. C. & Tilton, R. F. (1987). *J. Appl. Cryst.* **20**, 130–132.
Diederichs, K. & Karplus, P.A. (1997). *Nature Struct. Biol.* **4**, 269–275.
Dorsey, N. E. (1940). Editor. *The Properties of Ordinary Water Substance.* New York: Reinhold.
Dowell, L. G. & Rinfret, A. P. (1960). *Nature* (*London*), **188**, 1144–1148.
Engh, R. A. & Huber, R. (1991). *Acta Cryst.* A**47**, 392–400.
Esnouf, R. M., Ren, J., Garman, E. F., Somers, D. O., Ross. C. K., Jones, E. Y., Stammers, D. K. & Stuart, D. I. (1998). *Acta Cryst.* D**54**, 938–953.
Flack, H. D. & Bernardinelli, G. (1999). *Acta Cryst.* A**55**, 908–915.
Flack, H. D. & Bernardinelli, G. (2000). *J. Appl. Cryst.* **33**, 1143–1148.
Haas, D. J. & Rossmann, M. G. (1970). *Acta Cryst.* B**26**, 998–1004.
Hardman, K. D., Wood, M. K., Schiffer, M., Edmondson, A. B. & Ainsworth, C. F. (1971). *Cold Spring Harbor Symp. Quant. Biol.* **36**, 271–276.
Harp, J. M., Timm, D. E. & Bunick, G. J. (1997). Annu. Meet. Am. Crystallogr. Assoc., Abstracts WeB01 and P205.
Harp, J. M., Timm, D. E. & Bunick, G. J. (1998). *Acta Cryst.* D**54**, 622–628.
Hodel, A., Kim, S.-H. & Brünger, A. T. (1992). *Acta Cryst.* A**48**, 851–858.
Hope, H. (1988). *Acta Cryst.* B**44**, 22–26.
Hope, H., Frolow, F., von Böhlen, K., Makowski, I., Kratky, C., Halfon, Y., Danz, H., Webster, P., Bartels, K. S., Wittman, H. G. & Yonath, A. (1989). *Acta Cryst.* B**45**, 190–199.
Johari, G. P., Hallbrucker, A. & Mayer, E. (1996). *Science*, **273**, 90–92.
Kalb, A. J., Yariv, J., Helliwell, J. R. & Papiz, M. Z. (1988). *J. Cryst. Growth*, **88**, 537–540.
Kearsley, S. J. (1989). *Acta Cryst.* A**45**, 208–210.
Kleywegt, G. J. (2000). *Acta Cryst.* D**56**, 249–265.
Kriminski, S., Caylor, C. L., Nonato, M. C., Finkelstein, K. D. & Thorne, R. E. (2002). *Acta Cryst.* D**58**, 459–471.
Low, B. W., Chen, C. C. H., Berger, J. E., Singman, L. & Pletcher, J. F. (1966). *Proc. Natl Acad. Sci. USA*, **56**, 1746–1750.
McRee, D. E. (1992). *J. Mol. Graph.* **10**, 44–46.
Mayer, E. (1985). *J. Appl. Phys.* **58**, 663–667.
Mishima, O., Calvert, L. D. & Whalley, E. (1984). *Nature* (*London*), **310**, 393–395.
Mishima, O., Calvert, L. D. & Whalley, E. (1985). *Nature* (*London*), **314**, 76–78.
Mishima, O. & Stanley, E. (1998). *Nature* (*London*), **396**, 329–335.
Mitchell, E. P. & Garman, E. (1994). *J. Appl. Cryst.* **27**, 1070–1074.
Narten, A. H., Venkatesh, C. G. & Rice, S. A. (1976). *J. Chem. Phys.* **64**, 1106–1121.
Parkin, S. (1993). PhD thesis. University of California, Davis, USA.
Parkin, S. (1996). *PROTROT. Best-fit Superposition by the Quaternion Method.* Unpublished program.
Parkin, S. & Hope, H. (1998). *J. Appl. Cryst.* **31**, 945–953.
Parkin, S., Rupp, B. & Hope, H. (1996*a*). *Acta Cryst.* D**52**, 18–29.
Parkin, S., Rupp, B. & Hope, H. (1996*b*). *Acta Cryst.* D**52**, 1161–1168.
Pelletier, H. & Kraut, J. (1992). *Science*, **258**, 1748–1755.
Perrakis, A., Sixma, T. K., Wilson, K. S. & Lamzin, V. S. (1997). *Acta Cryst.* D**53**, 448–455.
Read, R. J. (1986). *Acta Cryst.* A**42**, 140–149.
Reeke, G. N. Jr, Becker, J. W. & Quiocho, F. A. (1971). *Cold Spring Harbor Symp. Quant. Biol.* **36**, 277–284.
Rodgers, D. W. (1994). *Structure*, **2**, 1135–1140.
Rodgers, D. W. (1997). *Methods Enzymol.* **276**, 183–203.
Scherrer, P. (1918). *Nachrich. Gesellschaft Wiss. Göttingen*, pp. 98–100.
Schick, B. & Jurnak, F. (1994). *Acta Cryst.* D**50**, 563–568.
Sheldrick, G. M. (2001). *XPREP* in *SHELXTL* (Linux Version 6.0). Bruker AXS Inc., Madison, Wisconsin, USA.
Sheldrick, G. M. (1997). *SHELXWAT* and *SHELXL*93. University of Göttingen, Germany.
Suzuki, Y. & Mishima, O. (2000). *Phys. Rev. Lett.* **85**, 1322–1325.
Teeter, M. M. & Hope, H. (1986). *Ann. NY Acad. Sci.* **482**, 163–165.
Terwilliger, T. C. (2000). *Acta Cryst.* D**56**, 965–972.
Terwilliger, T. C. (2001). *Acta Cryst.* D**57**, 1763–1775.
Tilton, R. F. Jr, Dewan, J. & Petsko, G. A. (1992). *Biochemistry*, **31**, 2469–2481.
Velikov, V., Borick, S. & Angell, C. A. (2001). *Science*, **294**, 2335–2338.
Weik, M., Kryger, G., Schreurs, A. M. M., Bouma, B., Silman, I., Sussman, J. L., Gros, P. & Kroon, J. (2001). *Acta Cryst.* D**57**, 566–573.
Wlodawer, A., Walter, J., Huber, R. & Sjölin, L. (1984). *J. Mol. Biol.* **180**, 301–329.
Yeh, J. & Hol, W. G. J. (1998). *Acta Cryst.* D**54**, 479–480.